ACS APPLIED MATERIALS & INTERFACES

www.acsami.org Research Article

Bioscaffold Stiffness Mediates Aerosolized Nanoparticle Uptake in Lung Epithelial Cells

Austin H. Williams, Adrien M. Hebert, Robert C. Boehm, Mary E. Huddleston, Meghan R. Jenkins, Orlin D. Velev,* and M. Tyler Nelson*

Cite This: *ACS Appl. Mater. Interfaces* 2021, 13, 50643−50656 Read Online

ACCESS | Metrics & More | Article Recommendations | Supporting Information

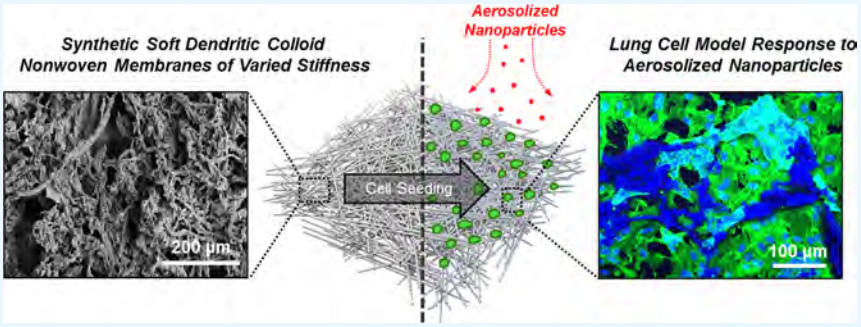

ABSTRACT: In this study, highly porous, ultrasoft polymeric mats mimicking human tissues were formed from novel polyurethane soft dendritic colloids (PU SDCs). PU SDCs have a unique fibrillar morphology controlled by antisolvent precipitation. When filtered from suspension, PU SDCs form mechanically robust nonwoven mats. The stiffness of the SDC mats can be tuned for physiological relevance. The unique physiochemical characteristics of the PU SDC particles dictate the mechanical properties resulting in tunable elastic moduli ranging from 200 to 800 kPa. The human lung A549 cells cultured on both stiff and soft PU SDC membranes were found to be viable, capable of supporting the air−liquid interface (ALI) cell culture, and maintained barrier integrity. Furthermore, A549 cellular viability and uptake efficiency of aerosolized tannic acid-coated gold nanoparticles (Ta−Au) was found to depend on elastic modulus and culture conditions. Ta−Au nanoparticle uptake was twofold and fourfold greater on soft PU SDCs, when cultured at submerged and ALI conditions, respectively. The significant increase in endocytosed Ta−Au resulted in a 20% decrease in viability, and a 4-fold increase in IL-8 cytokine secretion when cultured on soft PU SDCs at ALI. Common tissue culture materials exhibit super-physiological elastic moduli, a factor found to be critical in analyzing nanomaterial cellular interactions and biological responses.

KEYWORDS: *substrate stiffness, endocytosis, engineered materials, cell culture, nanoparticles*

1. INTRODUCTION

Tissue cultured polystyrene (TCPS) and polyester membrane Transwell inserts (TW) are ubiquitiously utilized as cell culture substrates due to ease of use and availability. These substrates, however, are more than a million-times stiffer that human tissues, and lack physiologically relevant tissue level microstructures and morphologies.[1] *In vitro* models representing the respiratory tract aim to provide a cost-effective, rapid, and simple platform to evaluate the toxicity of nanomaterials (NM). Due to the rapid commercial adoption and inadvertent production of NM byproducts, the potential for human exposure poses a serious health concern.[2−4] TCPS and TW are commonly used as cell culture substrates for *in vitro* NM toxicity assessment. The extrapolation of *in vitro* results to animal or human exposure standards often lacks correlation, reducing their relevancy.

Advanced *in vitro* systems aim to close the gap between the shortcomings of common *in vitro* platforms and complex *in vivo* models by incorporating tissue level complexities in a controlled cell culture environment.[5−14] These systems integrate aspects of tissue relevant microstructure,[15−18] morphology,[19−21] and mechanics.[22−27] Previous research efforts have utilized silicone scaffolds with moduli as low as 1−3 MPa, but no one reported the use of fibrous cell scaffolds with physiological elastic moduli below 1 MPa.[28] Physiological scaffolds for cell growth mimic the extracellular matrix (ECM) characteristics of human tissues: soft, three-dimensional and composed of highly fibrous components. Together, these parameters comprise a porous biocomposite material that is ideal for cell growth.[29−31] The

Received: May 28, 2021
Accepted: October 6, 2021
Published: October 20, 2021

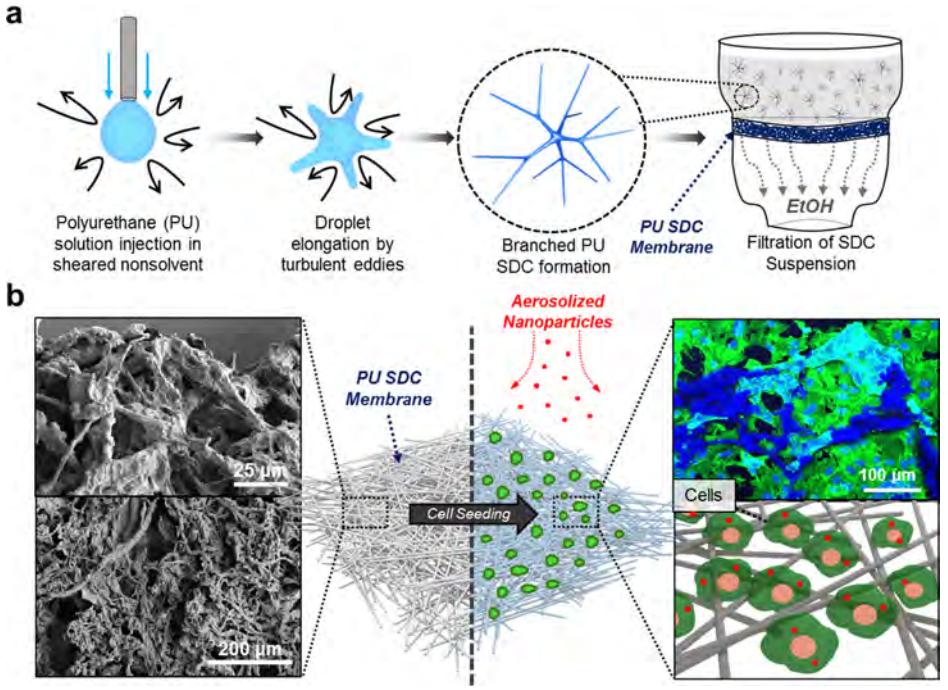

Figure 1. Schematic of soft dendritic colloid nonwoven preparation and administration of aerosolized NM on seeded nonwovens. (a) Process of PU SDC fabrication and nonwoven preparation includes multiple steps resulting in a mechanically robust mat for cell culture. (b) Left, scanning electron microscope images illustrating membrane morphology; middle—schematic representation of aerosol exposure of cells cultured on Soft or Stiff PU SDC membranes; right top—displays a confocal image of A549 human lung epithelial cells (green—phalloidin 488; blue—DAPI) grown on Soft PU SDC scaffolds to confluence at air−liquid interface (ALI) forming a tight air−liquid barrier; right bottom—displays a schematic of cellular integration within and on-top of the PU SDC resulting in a confluent, epithelial barrier capable of maintaining ALI culture conditions.

biomechanical properties of the ECM play a role in regulating cell behavior.[32,33] The dimensionality of the cell scaffold as well as the degree of pore isotropy is known to affect human cell proliferation, differentiation, and toxicity. Porous 3D scaffolds yield a more physiologically relevant topography and anisotropy.[34−37] The stiffness of the scaffolds has been shown to influence cell mechanotransduction pathways including human mesenchymal and endothelial cell models on 2D substrates.[38−46] For this reason, the development of biomimetic scaffolds with tunable mechanics from the same base material could serve as a superior platform for evaluating cellular responses, such as NM toxicity.

Herein, we investigate a new class of nonwoven cell scaffold materials named soft dendritic colloids (SDCs). The SDCs are made from micro- and nanofibrillar polyurethane (PU), *via* a process which enables control over their constitutive fiber size by modulating nonsolvent viscosity.[47] Such SDCs can be formed into cell culture membranes emulating the mechanical and morphological characteristics of human lung tissue. The SDC cell scaffolds were utilized in this study to develop a novel biomimetic *in vitro* lung inhalation model for nanomaterial toxicological testing. Cellular endocytosis and cytotoxicity of A549 human lung epithelial cells grown on 3D Stiff or Soft PU SDC membranes were compared to non-physiologically stiff 2D Transwell inserts. The cell cultures were exposed to Ta−Au nanoparticles (NPs) under submerged or air−liquid interface (ALI) conditions (Figure 1) as a baseline characterization of cellular responses to a common bioinert material. We aimed to gain a deeper understanding of the impact of culture condition and substrate physiochemical characteristics for *in vitro* model NM toxicological assessment or other biological applications.

2. MATERIALS AND METHODS

2.1. Fabrication of Polyurethane SDCs. A 3% (w/w) solution of polyurethane (PU, Huntsman Irogran PS455-203) was prepared in chloroform (Sigma-Aldrich) at 90 °C while stirred. Following dissolution, the PU solution was brought to room temperature and injected into the shear zone of a modified colloidal mill (IKA Magic Lab) at 20,000 rpm circulating turbulently sheared nonsolvent medium composed of ethanol (EtOH, Koptec) and glycerol (Gly, Alfa Aesar) to produce SDCs. The resulting polyurethane SDCs in suspension were then centrifuged for 2 min at 3.0 rcf and washed by redispersion in pure ethanol (8× dilution of SDC pellet volume). This process was repeated 5× to remove remaining glycerol and chloroform from the suspension.

2.2. Preparation of Polyurethane SDC Nonwovens. Nonwoven SDC membranes were prepared by filtering a 1.0% (w/w) PU SDC suspension in ethanol using a vacuum filtration apparatus (Millipore, HVLP 0.45 μm filter). Following filtration and drying, the membranes were peeled from the filter. The volume of PU SDC suspension deposited was adjusted such that the resulting membranes had thicknesses of ∼400 μm.

2.3. Mechanical and Optical Characterization of PU SDCs and Membranes. Polyurethane dendricolloids and SDC membranes were visualized using both optical microscopy (Olympus BX-61) and field emission scanning electron microscopy (FEI Verios 460L SEM). The membrane thickness was determined using a handheld micrometer (Marathon). Mechanical characterization of the membranes was performed using a universal testing machine (Instron 5943).

2.4. Cell Seeding and Maintenance. Human lung adenocarcinoma alveolar type-II like cell line, A549, was purchased from ATCC (ATCC CCL-185). Cells were expanded in Rosewell Park Memorial Institute (RPMI) 1640 growth medium (Hyclone, GE Health, USA) supplemented with 10% heat inactivated fetal bovine serum (HI-FBS, Gibco Inc., InVitrogen Inc., USA) and 1% penicillin/streptomycin (P/S, Millipore-Sigma Corp., USA). Cells were maintained under a humidified atmosphere of 5% CO_2 at 37 °C. 0.4 μm porous, polyester membrane Transwell (TW) devices of 12-well size, or engineered soft or stiff porous PU SDC substrates fitted into cell grown holders (Sigma-

https://doi.org/10.1021/acsami.1c09701
ACS Appl. Mater. Interfaces 2021, 13, 50643−50656

Aldrich) were utilized as cell culture substrates. Prior to cell culture, all substrates were soaked in ethanol containing an anti-fungal reagent (Fungin, Invivogen) for 24 h at room temperature. Subsequently, the scaffolds were washed thoroughly with phosphate buffered saline (PBS, Gibco) and coated with 100 μg/mL Collagen Type I (Advanced Biomatrix, Inc.) solution in PBS for 24 h at 4 °C. Prior to cell inoculation, the membranes were washed with a warmed complete medium to remove residual ECM coating solution. At a concentration of 3.5×10^5 cells/mL, each scaffold type (TW, Soft SDC, Stiff SDC) was inoculated under submerged conditions for five days with medium changes every 2 days. ALI culture conditions were achieved following expansion of the cells on the substrates (submerged culture), by removing the apical, epithelial compartment cell culture medium. ALI maintenance medium was added to basolateral compartment of the multiwell culture plate at a volume of 1 mL. Cells were cultured at ALI for additional five days, a total of 10 days from initial inoculation (5 days at submerged culture conditions). Submerged experimental samples were maintained under submerged conditions (100 μL apical surface and 1200 μL of cell culture medium in the basolateral compartment) for the full 10 days, maintaining a similar timeline to the ALI experimental conditions.

Images of A549 cells cultured on soft or stiff PU SDCs were collected to evaluate cell adhesion and morphology qualitatively. PU SDCs collected onto microscope coverslips were coated with collagen type I solution as previously stated, and subsequently inoculated with A549 cells. For imaging purposes, the cells were fixed in 4% paraformaldehyde (PFA, Electron Microscopy Inc.) diluted in isotonic phosphate buffer for 10 min at room temperature. The fixed cells were then washed twice with PBS, and immediately permeabilized using 0.1% triton-X solution (Fisher Scientific) in PBS containing 2% bovine serum albumin (BSA, ThermoFisher) at room temperature for 45 min. After permeabilizing, the cells were washed with PBS containing 2% BSA. Cells were then stained for f-actin (cytoskeleton) using an Alexfluor—488 conjugated phallodin dye (Actin Green, ThermoFisher) and the nuclei, DAPI (4′,6-diamidino-2-phenylindole, ThermoFisher). The stained coverslips were mounted to microscope slides and imaged using confocal microscopy (Nikon, Ti2 scanning confocal microscope, Nikon Inc.).

2.5. Paracellular Cascade Blue Transport. Paracellular transport of cascade blue (MW = 3 kDa, Catalog no. D7132, Invitrogen, USA) was used to assess barrier integrity. While TEER is often utilized to ensure that the integrity of the monolayer was maintained during the course of the experiment, this technique is inherently challenging to conduct between different scaffold materials as the baseline resistance is very different due to material properties, scaffold porosity, and morphology. Before each experiment, the culture medium was removed from the basolateral compartment and the monolayer was washed twice with warm HBSS (37 °C), for samples cultivated at ALI the surface was washed. To measure the permeability in the apical-to-basolateral direction, 1.5 mL of pre-warmed RPMI1640 culture medium was placed in the basolateral compartment. Cascade blue at 50 μg/mL in HBSS was then added to the apical chamber. To measure the transport, a sample was collected after 24 h of incubation from both the apical and basolateral compartments. A standard curve of cascade blue in HBSS and RPMI-1640 culture medium was utilized to convert a fluorescent plate reader (400 ex., 425 em.; Cytation 5, BioTek, USA) relative fluorescent units (RFU) to μg/mL. Cascade blue concentrations in the basolateral compartment were calculated and plotted as a function of time. Permeability coefficients, Papp, were calculated using the equation: $P_{app} = ((dC/dt)V)/(AC_0)$, where dC/dt is the slope of a linear fit to concentration *vs* time plot, V is the volume of HBSS in the receiver chamber, A is the surface area of the membrane (0.33 cm^2), and C_0 is the concentration of fluorescein added to the donor (apical) compartment (50 μg/mL).

2.6. VitroCell Cloud Aerosol Exposure. Ta−Au particles were purchased from Nanocompsix Inc. at a concentration of 1 mg/mL. Submerged exposures were carried out by adding Ta−Au to complete cell culture medium and subsequently vortexing the solution at high speed for 1 min. Following mixing, an aliquot was collected and measured using dynamic light scattering (DLS, Malvern Zetasizer) to ensure nanomaterial size and uniformity. Submerged exposures of Ta−Au NP were conducted by first creating a suspension in RPMI complete medium at a concentration of 5 μg/mL (0.5 mL volume). Ta−Au laden medium was added to the apical compartment of the TW or SDC cell culture substrates for 24 h.

The deposition of aerosolized Ta−Au NP was conducted using a VitroCell Cloud (VitroCell, Hamburg, Germany) system. First, the VitroCell Cloud unit was wiped down with 70% ethanol (Gibco, USA) and allowed to dry inside a laminar flow biosafety cabinet. The metal base was warmed to 37 °C. The wells were filled with warmed cell culture medium and fitted with the respective TW or soft or stiff SDC scaffolds seeded with A_{549} cells and matured at ALI. In a control well, a bare TW coated with polydimethylsiloxane (PDMS, Sylgard 184, Dow Corning, USA) was submerged in 200 μL of Di H_2O. Aerosolized NPs collected in the water provided a quality control for each exposure trial and a baseline of comparison for analysis of deposition efficiency using inductively coupled plasma−mass spectrometry (ICP−MS). Prior to experimental exposure, an analysis and optimization of Ta−Au NP aerosol exposure was conducted to determine final dosing concentrations (Supporting Information Figure S1, Vitrocell Cloud Ta−Au NP dosimetry analysis). 691 μL of Ta−Au NP solution (1 mg/mL in Di H_2O) was added to 9 μL of 1:80 phosphate buffered saline (PBS), and subsequently added to the loading port of the nebulizer. Aerosolization occurred for 30−45 s, creating a dense NP cloud within the VitroCell Cloud cell culture housing. Control samples were isolated and exposed to a cloud of similar PBS concentration as represented in the Ta−Au NP exposure. A settling period of 5 min was found to be sufficient to achieve maximal particle deposition. After deposition, TW or SDC cell culture samples were moved back to cell culture plates and incubated for 24 h.

2.7. Cell Viability Assessment. 50 μL of supernatant from the apical (100 μL of stock cell culture medium was added to apical surfaces of ALI samples and allowed to incubate for 30 min before removing 50 μL for LDH analysis) and basolateral (42 μL of conditioned ALI basolateral medium was isolated and diluted with stock cell culture medium to a final volume of 50 μL to account for the 1.2-fold dilution factor) compartment of each sample was isolated and plated in triplate in a 96 well plate. 50 μL of LDH assay buffer (Membrane Integrity Assay, Promega, USA) was mixed with each sample and incubated at 37 °C for 2 h. A lysis cell suspension positive control was utilized to confirm assay functionality. LDH assays were evaluated using a fluorescent plate reader (Cytation 5, Biotek, USA) set to an excitation/emission wavelength of 569/590 nm, respectively. While LDH analysis is a well-established method to evaluate cellular necrosis, it is an indirect measure of individual cell death. Therefore, after 24 h of incubation, cells were trypsinized from the scaffolds, centrifuged, and resuspended in 1 mL of warm PBS for individualized flow cytometry-based viability assessment. A 100 μL aliquot was taken from the cell suspension and mixed in 1:1 ratio with cell exclusion viability assay buffer (Guava Viacount, Millipore, USA) and incubated for 5 min. The stained cells were then processed using a Guava Easycyte 12-HT (Millipore, USA) microfluidic flow cytometer acquiring 5000 reads in technical duplicate per sample (Supporting Information Figure S2, a cell count per scaffold material). Lysed cells were utilized as a negative control for gating purposes. The total cell count and total percent viable cell fraction were determined. The total cell count was also used to normalize LDH, IL-8 cytokine secretion, and ICP−MS results.

2.8. ICP−MS Nanoparticle Uptake Analysis. A549 cells were released from their respective membranes, washed, centrifuged into a pellet, and digested in 1 mL of 50% nitric acid (analytical grade >99.9% purity, Sigma-Aldrich, USA) at 97 °C for 16 h. The digested cellular and uptaken nanoparticle acid solution was vortexed at 10,000 rpm for 2 min (VBR, USA), and then diluted into 10 mL of double distilled water. 2% internal standard (PerkinElmer, USA) was added to each of the samples, and the standard curve was developed using serial dilution of Ta−Au in 50% nitric acid diluted 10-fold in ddiH_2O. Standards were calculated after every five samples for quality control. All samples were run using an autofed- ICP−MS unit (ICP−MS 300D, PerkinElmer, Waltham, MA). Values were converted using the standard curve and internal standards and reported as gold μg/mL per 10^5 cells.

https://doi.org/10.1021/acsami.1c09701
ACS Appl. Mater. Interfaces 2021, 13, 50643−50656

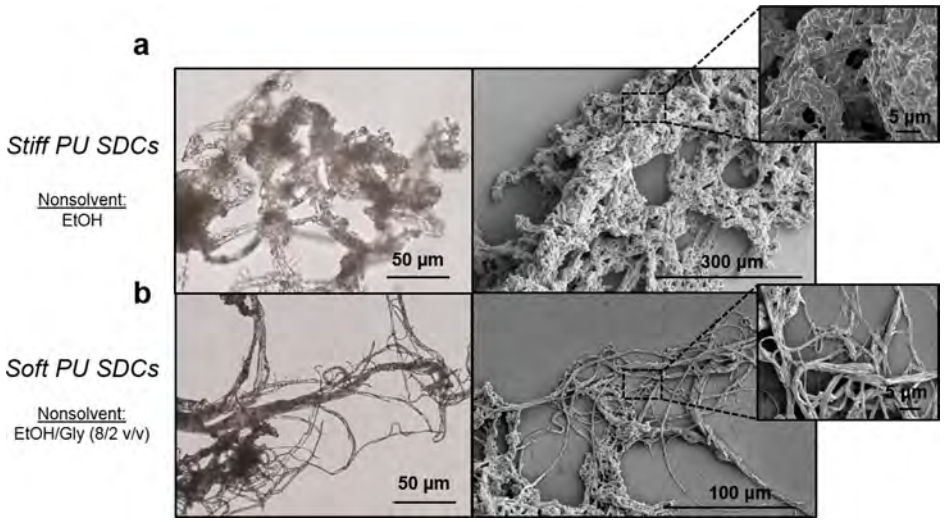

Figure 2. Glycerol acting as a non-solvent provides polymer processing control over the morphology of the Soft and Stiff PU SDC mats. Optical and scanning electron micrographs of PU SDCs prepared with (a) 100% EtOH and (b) 80/20 EtOH/Glycerol (v/v) nonsolvents. The addition of just 20 vol % glycerol to the nonsolvent medium reduces the resulting fiber size in the produced SDC.

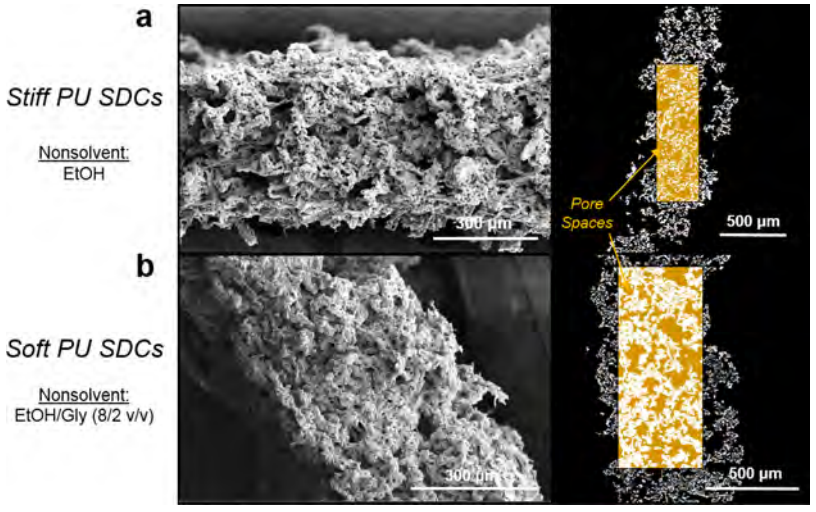

Figure 3. Morphological characterization of Stiff and Soft PU SDC nonwovens. Analysis of PU SDC membranes by scanning electron microscopy (left) and X-ray nanotomography (right) of samples prepared using nonsolvents composed of (a) 100% EtOH (Stiff PU SDCs) and (b) 80/20 (v/v/) EtOH/Gly (Soft PU SDCs). Highlighted portions within the membranes indicate how porosity data was calculated from 3D reconstructions.

2.9. Interlukin-8 (IL-8) Cytokine Secretion. Effluent from the basolateral compartment of TW or Soft or Stiff PU SDC tissue models was collected post-24 h of exposure and snap frozen for future use. IL-8 pro-inflammatory cytokine secretion was measured using an enzyme linked immune-sorbent assay (Human IL-8 ELISA MAX, Biolegend Inc., USA) following manufacturers protocols. Briefly, 100 μL of a cell culture effluent (83 μL of conditioned ALI basolateral medium was isolated and diluted with stock cell culture medium to a final volume of 100 μL to account for the 1.2-fold dilution factor) was added to capture antibody coated wells of a 96-well plate in triplicate format. Between each step, four detergent washes [0.1% Triton-X 100 in phosphate buffered saline (PBS), Thermo-Fisher Scientific, USA] were administered and the plate was subsequently pat dried on to a paper towel to limit non-specific binding effects. Detection antibody, followed by streptavidin, and running buffer were added to each of the wells and the absorbance was read at 450 nm (Biotek Cytation 5, Biotek, USA). Experimental samples were converted using a standard curve, and the data were presented as the mean ± standard error in pg/mL per 1×10^5 cells. 200 μL of Lipopolysacchride (LPS, *E. coli* 026:B6 origin, eBioscience, Invitrogen, USA, Cat. # 00-4976-93) solution at 100 μg/mL was added to the apical compartment of TW or PU SDC samples for submerged culture condition. ALI samples were exposed in the basolateral compartment using a volume of 1.5 mL for 24 h.

2.10. Statistical Analysis. Statistical significance was determined using a two-way analysis of variance (2-way ANOVA) with significance level of 0.05. Post-hoc analysis of differences was evaluated using a Tukey analysis to determine significant differences between variables. All statistical and graphical analysis was conducted using GraphPad Prism 8.4 (GraphPad, USA). Significance markers and accompanying tests are identified in the figure legends.

3. RESULTS

3.1. Morphology of Polyurethane SDCs. Porous, ultra-soft polymeric membranes were prepared by first fabricating soft dendritic colloids (SDCs) from a biocompatible polyurethane (PU) using a pure ethanol (EtOH) nonsolvent as previously described (Figure 2a).[47] The resulting Stiff PU SDCs showed the characteristic branched-fibrous structure as the previously reported SDCs but had a more globular morphology with larger and more clustered fibers (Figure 1a). The addition of 20% vol. glycerol (Gly) to the ethanol nonsolvent during the formation

https://doi.org/10.1021/acsami.1c09701
ACS Appl. Mater. Interfaces 2021, 13, 50643−50656

process clearly resulted in Soft PU SDCs with more expressed fibers of smaller diameter (Figure 2b).

3.2. PU SDC Nonwovens Optical and Internal Structure Characterization. The SDCs are produced in suspension, hence, the resulting particles are easily assembled into mechanically robust nonwoven sheets of high porosity and surface area by layering. Following the particle washing step, PU SDC in EtOH suspensions are simply vacuum-filtered and dried to yield highly soft and elastic PU SDC membranes. Cross-sectional scanning electron micrographs of both PU SDC nonwovens (Figure 3) as well as the internal 3D structure enabled to measure the fraction of pore space of the PU SDC nonwovens using X-ray nanotomography. Because of the highly anisotropic shape of the pores in the SDC nonwovens, we analyzed the minimum, average, and maximum pore Feret diameters using Dragonfly software (Table 1, Supporting Information Video 9—micro-CT video of soft and stiff PU SDC scaffolds).

Table 1. Porosity and Pore Feret Diameters of Soft and Stiff PU SDC Nonwovens Analyzed Using Zeiss Xradia Micro-CT

	porosity (%)	min. feret diameter (μm)	avg. feret diameter (μm)	max. feret diameter (μm)
stiff PU SDC	70.09	207.77	1072.24	1891.87
soft PU SDC	70.23	282.22	1322.04	1662.87

When producing these ultrasoft polymer membranes, repeated-strain effects such as membrane creep and subsequent tensile modulus relaxation could be of concern. To investigate the mechanical resilience of both PU SDC membranes, a series of experiments were performed in which soft and stiff SDC membranes were subjected to cyclic strain, while the elastic moduli, as well as the magnitude of membrane creep, were recorded each strain cycle. A representative stress−strain curve for cyclic, 30% strain shows how these values drift in the course of undergoing cyclic strain (Figure 4a). The tensile moduli and membrane creep for soft and stiff PU SDC membranes were then evaluated using a cyclic strain ramp up to 50% strain for five cycles (Figure 4b,c). The stiff PU SDC membrane displays tensile moduli (~750 kPa) that are 3-fold larger than the soft PU SDC membranes (~250 kPa).

3.3. Substrate Stiffness-Dependent Nanoparticle Uptake. A baseline assessment of lung epithelial cell attachment, growth, establishment of ALI culture, and biological responses to an inert nanoparticle aerosol was conducted on biomimetic PU SDC scaffolds. While A549 cell culture on traditional TW substrates have been extensively characterized using imaging techniques, cell attachment and growth on PU SDC scaffolds have not been characterized. Figure 5 shows A_{549} cells adhered to and grew on stiff (Figure 5a) and soft (Figure 5b) PU SDC scaffolds for 4 days exhibit similar morphologies with limited cellular infiltration into the scaffold depth (additional 3D fluorescent confocal image reconstruction videos are made available in the Supporting Information section, Supporting Information files S6, S7, and S8). This was also confirmed by the establishment of the ALI condition, of which A_{549} cells maintained ALI without leakage on both stiff and soft PU SDC scaffolds as compared to TW cultures. Furthermore, Figure 6 depicts the apparent permeability of A_{549} cultures on TW and stiff or soft PU SDC scaffolds (Supporting Information Figure S3, scaffold only cascade blue transport). No significant

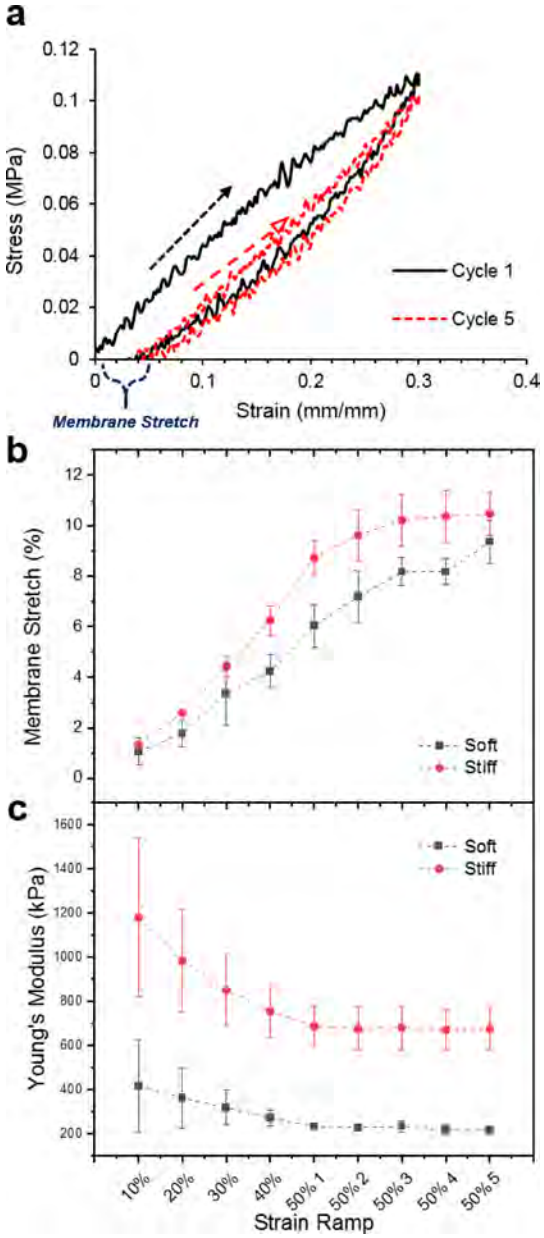

Figure 4. Mechanical properties of stiff and soft PU SDC membranes. (a) Representative cyclic PU SDC membrane strain indicating elastic modulus relaxation and membrane stretch after cyclic 30% strain. (b) Membrane creep and (c) elastic modulus of soft and stiff PU SDC nonwovens with ramping, indicating cycling strain up to 50% (n = 3). PU SDCs produced with smaller fibers result in softer nonwoven membranes.

difference in the flux of a 3 kDa Cascade blue fluorescent indicator was observed between scaffold types cultured under ALI conditions; however, the permeability was significantly decreased as compared to submerged conditions. Apparent permeability was significantly higher on soft PU SDC scaffolds when cultured under submerged conditions, suggesting the importance of ALI. A_{549} lung cells, cultured on traditional polyester TW substrates or engineered PU SDCs were exposed to Ta−Au NP. Lung epithelial cell culture was conducted both with cell culture medium covering the cells, or submerged condition, and with the cells exposed to air on the apical surface and liquid on the basolateral surface, or ALI condition, as indicated in Figure 7. Cells cultured in submerged conditions on

https://doi.org/10.1021/acsami.1c09701
ACS Appl. Mater. Interfaces 2021, 13, 50643−50656

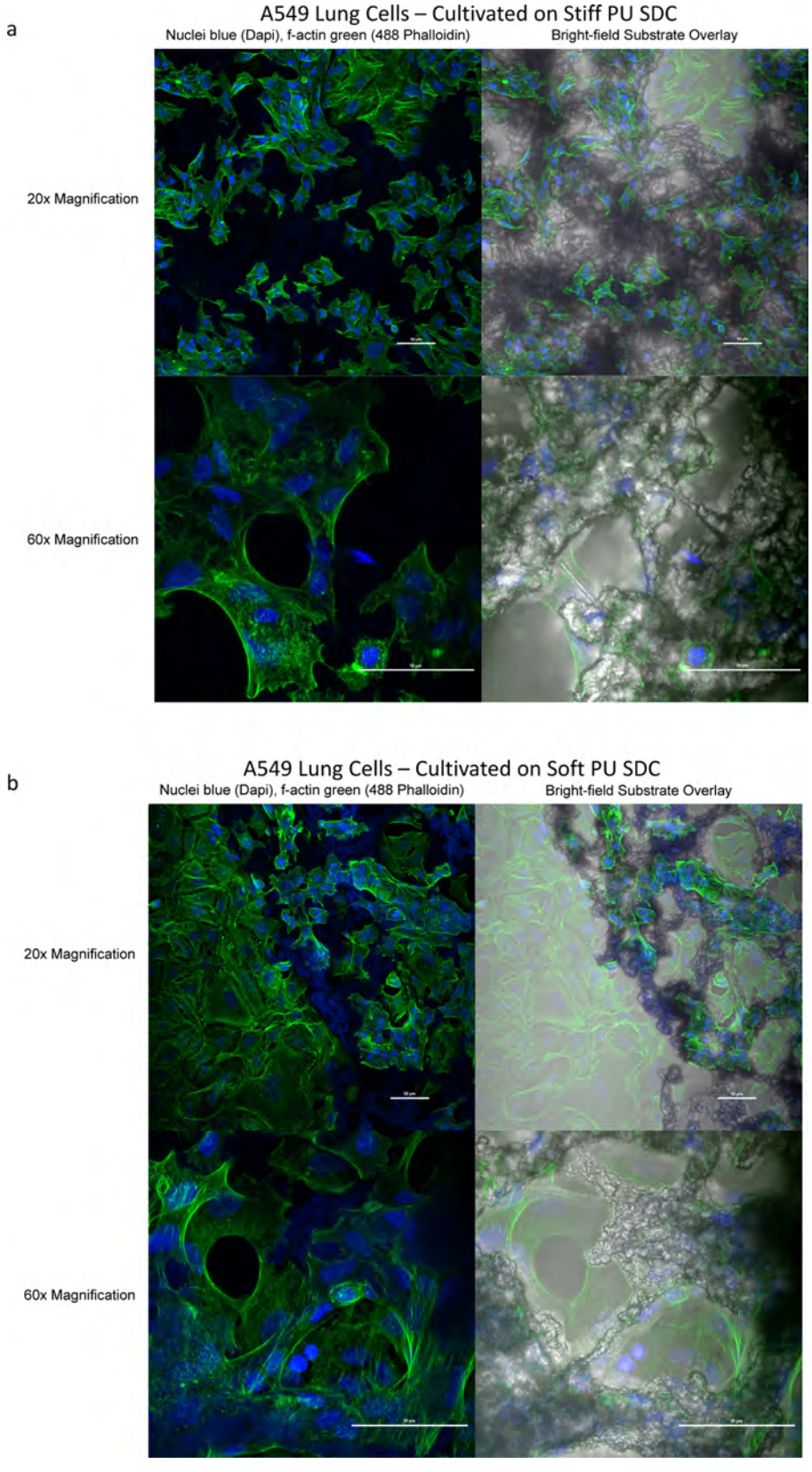

Figure 5. A_{549} cell attachment and growth on stiff and soft PU SDC scaffolds as depicted by confocal microscopy. A_{549} cells adhered and grew on stiff (a) and soft (b) PU SDC scaffolds for 4 days showing the development of confluent cell sheets, minimal cellular infiltration, and no significant differences in morphology (scale bars = 50 μm).

PU SDCs showed a 2-fold increase ($p < 0.05$, two-way ANOVA, post-hoc Tukey test) in Ta–Au NP uptake compared to TW substrates (Figure 7a). No difference in Ta–Au NP uptake was observed between soft or stiff PU SDC nonwovens for

https://doi.org/10.1021/acsami.1c09701
ACS Appl. Mater. Interfaces 2021, 13, 50643–50656

Figure 6. Apparent permeability (P_{app}) of A_{549} monolayers cultivated on TW, stiff or soft PU SDC scaffolds. The P_{app} of A_{549} monolayers cultivated on the different scaffolds and culture conditions (submerged *vs* ALI) were determined by measuring the paracellular flux of fluorescent cascade blue. (one-way ANOVA, post-hoc Tukey analysis, $p < 0.05$, * indicates statistical significance).

submerged culture conditions. Aerosol exposure to Ta−Au NP for A_{549} cells cultured at ALI resulted in elastic modulus-dependent increase in NP uptake with decreasing substrate stiffness. A_{549} uptake on stiff PU SDC membranes was 2-fold greater ($p < 0.01$, two-way ANOVA, post-hoc Tukey test) than TW, and for cell cultured on soft PU SDC membranes the uptake was 4-fold greater than TW ($p < 0.0001$, two-way ANOVA, post-hoc Tukey test). Furthermore, A_{549} cellular uptake of Ta−Au NP on soft PU SDC membranes was 2-fold greater than that of cells cultured on stiff PU SDCs (Figure 7b). In summary, substrate stiffness dependent Ta−Au NP uptake was observed for both culture conditions; however, differences in total uptake and stiffness sensitivity were observed with ALI culture conditions on the soft SDC substrate resulting in the highest NP uptake and cell sensitivity.

3.4. Cellular Viability and Cytokine Secretion. A_{549} cellular viability was assessed using flow cytometry (Figure 8a−c). Cells were isolated from traditional TW or PU SDC scaffolds post-24 h after submerged or after ALI Ta−Au aerosol exposure. No significant differences were observed for cells exposed on TW for either culture condition (Figure 8a). Likewise, no significant differences were detected for cells culture under submerged conditions on PU SDCs (Figure 8b). However, when cultured at ALI on Soft PU SDCs, a 20% decrease in viability (Figure 8c) was observed when exposed to Ta−Au as compared to cells cultured under similar conditions on TW or stiff PU SDC scaffolds.

Cytotoxicity was measured by quantifying the amount of lactate dehydrogenase (LDH) released from cells in response to Ta−Au exposure, culture condition, and substrate stiffness. While Ta−Au is not thought of being a toxic material, excessive endocytosis can elicit a cell stress response resulting in cell death. LDH is a cytosolic enzyme, which when released into the cell culture medium directly indicates a loss of cellular membrane integrity, or cytotoxicity. Flow cytometry directly measures live cell numbers, meaning dead cells are not captured in the sample due to damage or otherwise being lost in the medium would not be counted in the viability assessment providing an artificially high viability percentage. As seen in Figure 9, LDH activity in the apical (upper, epithelial compartment) or basolateral (lower, medium compartment) for submerged (SUB) or ALI TW culture conditions showed no statistical difference in LDH secretion. Conversely, A_{549} LDH activity increased in both the apical and basolateral compartments when exposed to Ta−Au at ALI while cultured on the Soft PU SDC mats.

Epithelial exposure to pathogens, virus, chemicals, or particulates such as NMs can cause significant damage or even death. Inflammatory cytokine secretion from lung cells signals local cellular stress to resident and circulating immune cells. IL-8 cytokine secretion is a hallmark stress marker and indicator of epithelial inflammation. IL-8 secretion was measured in the lower (basolateral) compartment of TW and PU SDC models

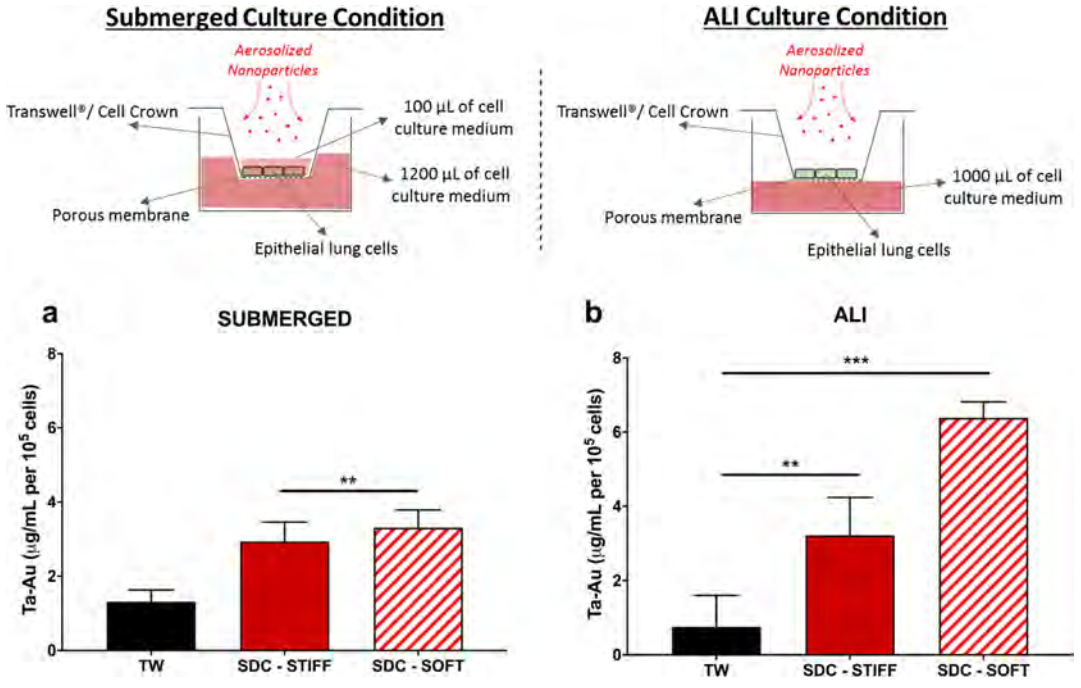

Figure 7. Impact of culture condition and substrate stiffness on Ta−Au nanoparticle uptake. Ta Au nanoparticle uptake measured by ICP−MS for A_{549} cells cultured on SDC-stiff or SDC-soft substrates was compared to traditional TW substrates for (a) submerged and (b) ALI culture conditions following 24 h of Ta−Au NP exposure. (one-way ANOVA, post-hoc Tukey analysis, $p < 0.05$, * indicates statistical significance).

https://doi.org/10.1021/acsami.1c09701
ACS Appl. Mater. Interfaces 2021, 13, 50643−50656

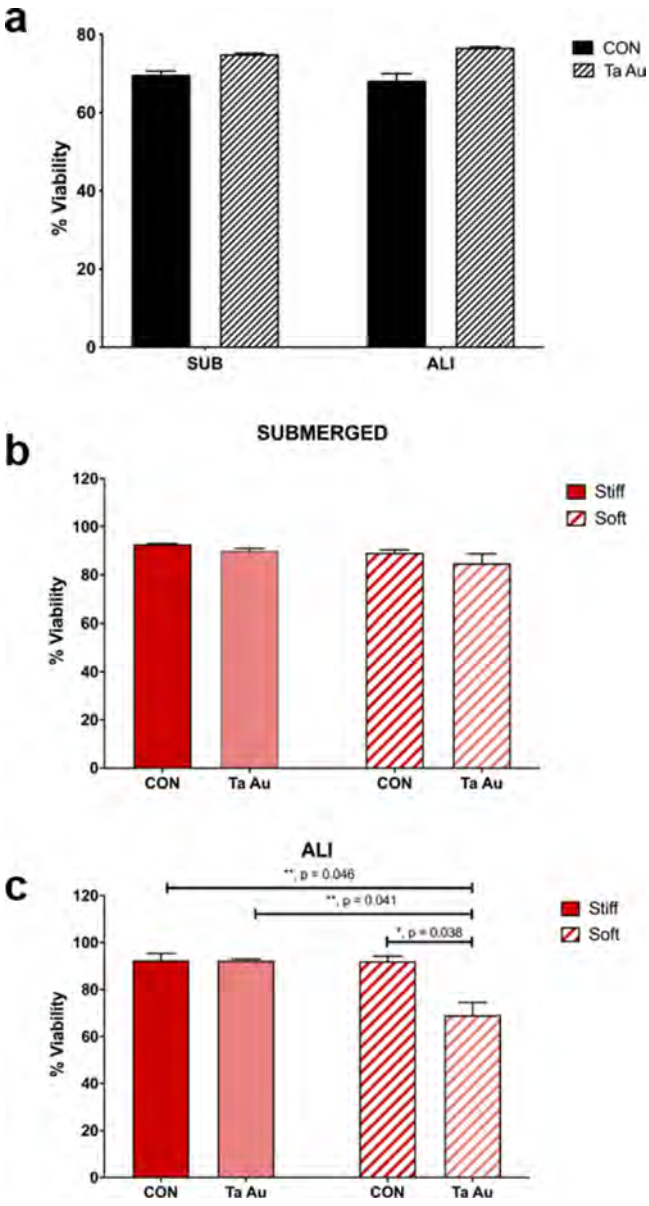

Figure 8. Impact of substrate stiffness and cultured condition on A_{549} viability in response to Ta−Au aerosol expsoure. The viability of A_{549} cells 24 h post-exposure on (a) TW both submerged and ALI, and on PU SDC membranes cultured at (b) submerged or (c) ALI conditions. (one-way ANOVA, post-hoc Tukey analysis, $p < 0.05$, * indicates statistical significance).

after Ta−Au exposure (Figure 10). No significant difference was detected for TW models IL-8 secretion when exposed to Ta−Au for either culture condition. Similarly, A_{549} response to Ta−Au exposure for submerged (Figure 10b) or ALI (Figure 10c) culture on Stiff PU SDCs showed no statistical difference. Conversely, a significant increase in IL-8 secretion was observed for cells cultured on soft PU SDCs for both submerged (Figure 10b) and ALI conditions (Figure 10c). IL-8 secretion was increased 3.8-fold with respect to no treatment on soft SDC substrates, and 2.2-fold as compared to cells cultured on stiff PU SDCs cultured submerged (Figure 10b). Likewise, a 3.7-fold increase was observed when cells cultured on soft PU SDC were exposed to Ta−Au at ALI, and a 2-fold increase when compared to cells cultured on stiff PU SDC scaffolds.

4. DISCUSSION

Biological research worldwide is slowly moving away from animal models and adopting *in vitro* methods. The need for physiologically relevant *in vitro* tissue models for toxicological or other biological assessments is in high demand. The emerging advanced models are diverse, ranging from commercially available full thickness, differentiated human tissues, to custom built tissue engineered models derived in single laboratories. There is a demand for better models and the ability to tailor tissue conditions for specific exposures or analyses. Commonly, a significant biomaterials challenge in the field is the dependency on structure−function relationships in materials that limit the ability of these materials to be tuned in their bulk state without altering other physiochemical parameters. Therefore, novel polymer processing techniques are needed that provide the ability to tune mechanics, microstructure, and morphology independently using the same bulk material, providing a high degree of tailoring. Here, we report a novel technique to create biomimetic polymeric scaffolds with tunable elastic modulus enabling physiological cell culture conditions for NM exposure analysis.

Shear-driven polymer precipitation is gaining traction as an innovative and versatile technique that can be used to manufacture tailored polymeric nanomaterials including micro-rods, nanofibers, SDCs, and thin sheet-like particles from both synthetic and biopolymer materials.[47−49] PU was selected in this study to produce biocompatible membranes due to its bulk material properties. PU is a thermoplastic polymer with lower melting temperature, low elastic modulus at room temperature, and compatible with wide range of organic solvents. In addition, PU is commonly used in medical devices due to is high degree of biocompatibility. The SDCs were produced in a rapid and scalable precipitation process (Figure 1). The interplay between the various mass transport phenomena involved in the SDC formation process are highly complex and not completely understood. These phenomena include the rate of polymer precipitation dictated by the chemical potential gradient between the solvent and nonsolvent phases as well as the hydrodynamic characteristics of the turbulent flow and injection solutions impacted by the viscoelasticities of the solvent and nonsolvent phases.[50] The addition of 20 vol % Gly to the EtOH nonsolvent affects the chemical potential gradient controlling the rate of polymer precipitation at the polymer−nonsolvent interface compared to that of a pure EtOH nonsolvent, but it also increases the viscosity of the nonsolvent nearly 5-fold.[51] Nevertheless, the PU SDCs prepared using EtOH as a nonsolvent exhibited thicker fibers than the previously reported SDCs composed of other synthetic polymers, yet had the same characteristic, branched fiber structure. Microscopy of these particulates reveals that these thicker fibers appeared to be similar to aggregated "braids" of smaller fibers (Figure 2). Overall, PU SDCs represent a novel fibrillar biomaterial with tailored microstructural and mechanical parameters necessary for emulating human physiology and biological responses.

While the control of fiber diameter displayed here is a common feature in both melt-blowing and electrospinning, shear-driven precipitation is a versatile technique which is capable of producing many additional, controlled particle morphologies beyond nanofibers including nanoscale sheet particulates and ribbons.[47] SDC nonwovens prepared from either type of PU SDC formed nonwovens that were cohesively connected by the SDC fiber sub-contacts (Figure 3). The

https://doi.org/10.1021/acsami.1c09701
ACS Appl. Mater. Interfaces 2021, 13, 50643−50656

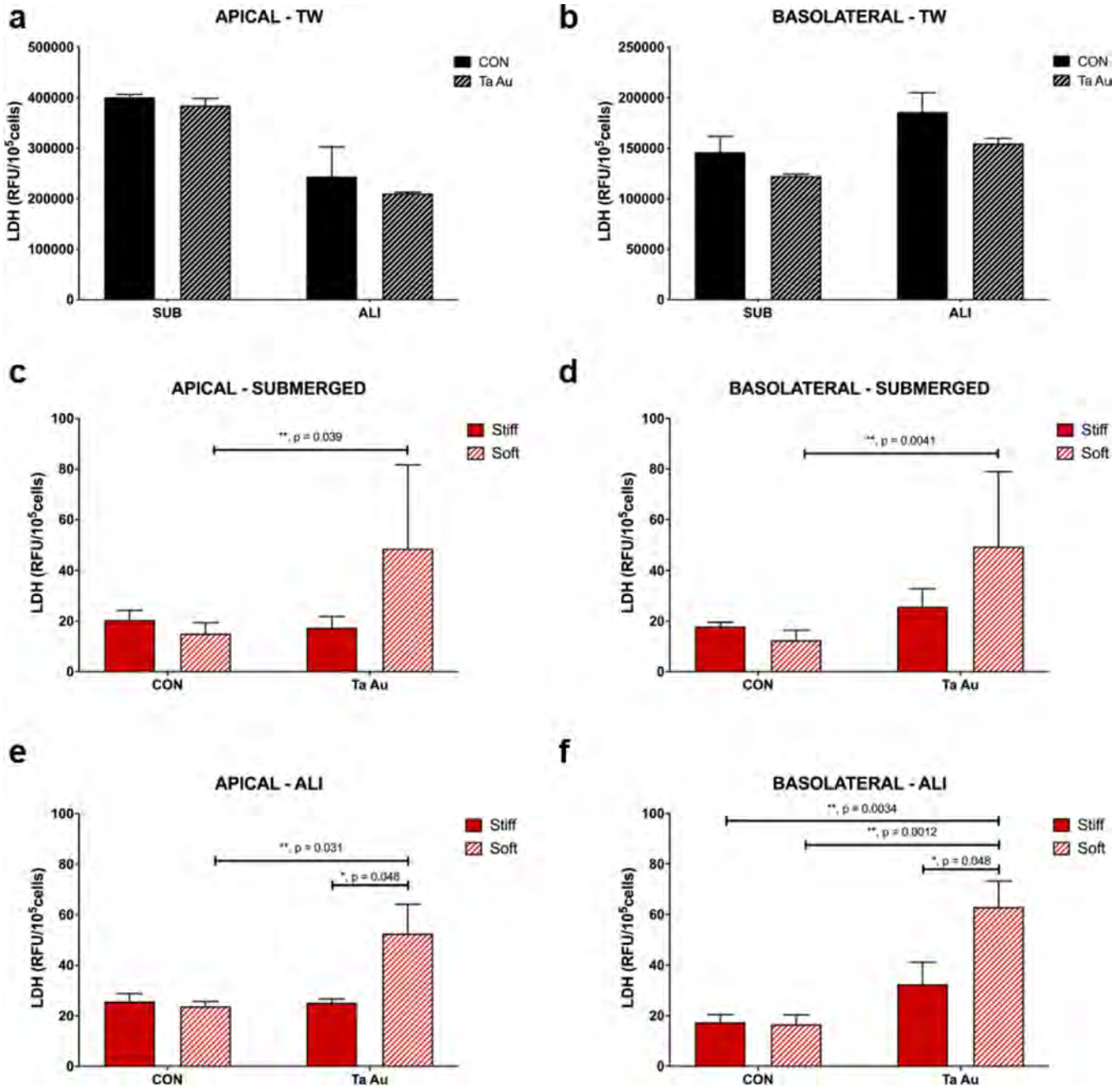

Figure 9. Impact of culture condition and substrate stiffness on A_{549} epithelial cell cytotoxicity. A_{549} LDH activity was assessed in the apical (left column) and basolateral (right column) compartments of TW (a,b), and soft and stiff PU SDC scaffolds for submerged (c,d) and ALI (e,f) culture conditions. (one-way ANOVA, post-hoc Tukey analysis, $p < 0.05$, * indicates statistical significance).

mechanical entanglement of the SDC fibers resulted in a robust and continuous mat with highly anisotropic pores in both geometry and size, offering a favorable environment for cell attachment and proliferation.[35,52] Analysis of the PU SDC membranes by X-ray nanotomography revealed that the soft and stiff PU SDC substrates had a pore volume of ~70%. This high porosity in PU SDC membranes may further benefit cellular response, as many similar nanofibrous membranes produced most commonly by electrospinning see decreased cell invasion and sub-optimal cell response due to the smaller pore size of electrospun nanofiber matrices.[31] X-ray nanotomography also allows visualization of the internal, disordered pore network of the nonwoven with features ranging from microns to hundreds of microns (Supporting Information Video S7, microCT video).

The analysis reveals that the pores of the soft SDC nonwovens exhibited a slightly higher average Feret diameter (1072 μm) than those composed of stiff SDCs (1322 μm) despite the smaller diameter of their fibrillar features (Table 1). While the size of the pores and the thickness of the membranes differs from that of human tissue and that of TW, the formation of ALI culture conditions and similar total cell counts suggests the PU SDC scaffolds supported the formation of monolayer barrier. This lung-blood barrier is crucial in maintaining human physiology and protection from systemic toxicant threats. Furthermore, TW membrane porosity is significantly lower than that of tissue or PU SDC membranes, and the stiffness as measured under tensile loading is nearly one million times higher ($E \sim 1.9-2.9$ GPa). These factors have been called out as

https://doi.org/10.1021/acsami.1c09701
ACS Appl. Mater. Interfaces 2021, 13, 50643−50656

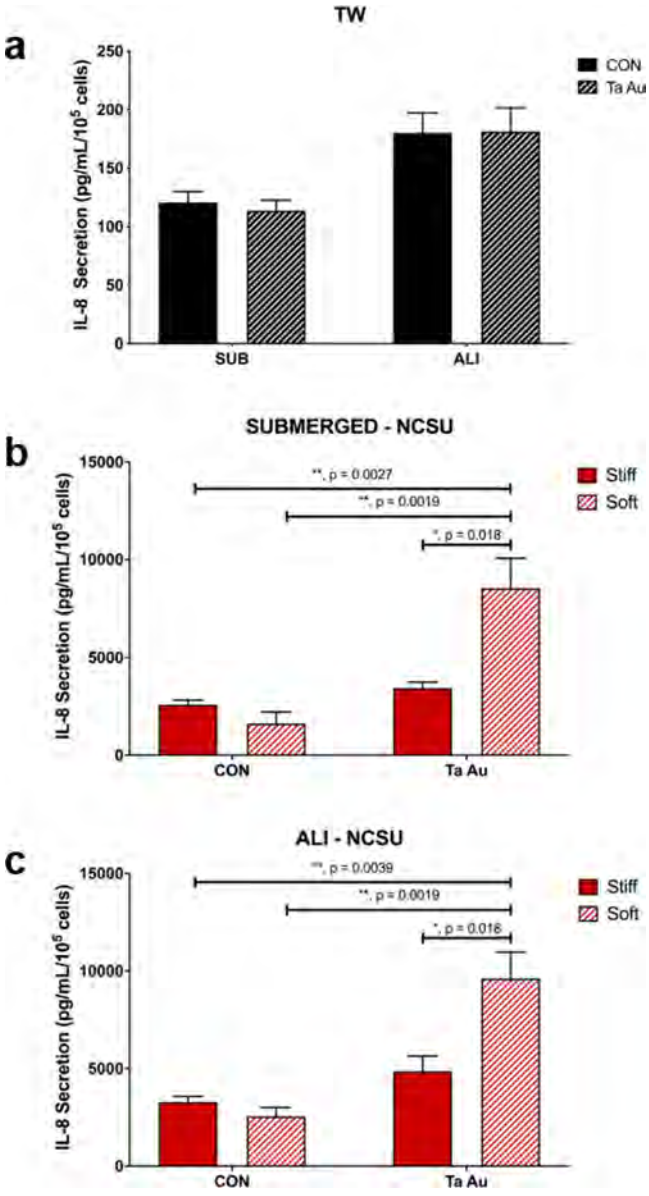

Figure 10. A_{549} cells cultured on soft PU SDCs displayed increased IL-8 cytokine secretion. IL-8 cytokine secretion from A_{549} cells cultured on TW (a) or PU SDCs cultured submerged (b) or at ALI (c) was measured from basolateral medium using ELISA. [one-way ANOVA, post-hoc Tukey analysis, $p < 0.05$, * indicates statistical significance. Supporting Information Figure S4—100 μg/mL lipopolysaccharide (LPS, *E. coli* origin) control].

challenges to overcome in the *in vitro* industry as they play a major impact on cellular responses. However, optimizing membrane porosity, thickness, microstructure and mechanics is not enough; there are the practical limitations of handling ultra-thin, soft, and highly porous membranes as they often lack structural and mechanical integrity for building model systems and mechanical actuating them for simulation of physiological forces. Additionally, previous research study has investigated similar cell behavior on substrates composed of woven polymeric fibers. Woven polymeric membranes, however, see aligned and consistent fiber and pore geometries that are not characteristic features of the branched, anisotropic architectures of physiological tissues. Polydimethylsiloxane (PDMS) substrates, as commonly used in microfluidic devices, have shown promise in being able to apply isotropic mechanical strain to human cultured cells including lung epithelial cells, simulating breathing forces. PDMS has a linear elastic modulus that varies with crosslinker concentration, resulting in a range of elastic moduli between 0.57 and 3.7 MPa. The lower limits of possible PDMS elastic moduli approach those reported in this effort, but lack porosity and the 3D dimensional composition of human tissue.[26] The PU SDCs described are a novel solution to developing mechanically robust, highly porous, biocompatible, and tunable substrates for future *in vitro* investigations of cellular biology, improvements in the thickness and reduction of pore size will further enhance these scaffolds potential.

The low elastic moduli of PU SDC nonwovens indicate that they are very soft materials with moduli below 1 MPa and surprisingly good mechanical integrity. After five cycles of 30% strain, representative stress−strain curves show that both soft and stiff PU membrane exhibited elastic modulus relaxation and some membrane creep, although the ability of SDC membranes to withstand 5 cycles of supraphysiological stress from 50% strain displayed the integrity of the SDC membrane as tissue substrates (Figure 4). Despite their identical chemical composition, the soft PU nonwovens exhibited much lower tensile moduli that leveled off at ∼200 kPa compared to the stiff PU membranes with moduli that reached ∼750 kPa (Figure 4c). Both the Soft and the Stiff PU SDC membranes exhibited tensile elastic moduli within the range of healthy (0.5−250 kPa, human lung) and diseased (50−900 kPa, human fibrosis) tissue, respectively.[53] Membrane elasticity similar to aligned or randomly oriented electrospun fiber mats decreased with increasing individual fiber diameter.[54] For both stiff and soft PU SDC nonwovens, the tensile moduli of membranes during the strain ramp were nearly 2× larger than those reached after the membranes underwent 50% cyclic strain. We hypothesize that the smaller fibers of the soft PU SDCs may form weaker networks that are more easily ruptured than those of the stiff PU SDCs.

The biocompatibility, softness, and porosity of the fibrillar SDC nonwovens makes them potentially valuable biomimetic cell scaffold materials for soft, physiological tissues.[55] Moreover, the tunability of the processing technique provides a means to selectively optimize scaffold mechanics and microstructure independent of chemistry, thus providing a consistent and controllable platform for biological investigations.[30] The inherent versatility in choice of polymer offered by the shear-driven precipitation technique enables the high-throughput development of similar SDC membranes produced from other polymers including biodegradable and bio-derived polymers. This allows for making substrates of tailored mechanical properties that can be used as tissue engineering bioscaffolds in addition to their utilization as synthetic tissue substrates to measure cell toxicology presented herein.[56,57]

NMs possess unique physiochemical characteristics differing from the bulk material.[4] Modifications in size, surface chemistry, charge, or shape can significantly alter a NM's impact on cellular responses. Due to NM's unique size, respiratory-tract inhalation is of concern and the rate of new development and adoption of NM has driven a need for rapid, greater throughput capabilities to test safety. NM *in vitro* respiratory toxicology has been commonly executed using common 2D, flat tissue culture models or hanging TW systems. Both tissue cultured polystyrene (TCPS) and TW polyester membranes are notoriously stiff. While scaffold biomechanics are often a major consideration for other pathological investigations,

https://doi.org/10.1021/acsami.1c09701
ACS Appl. Mater. Interfaces 2021, 13, 50643−50656

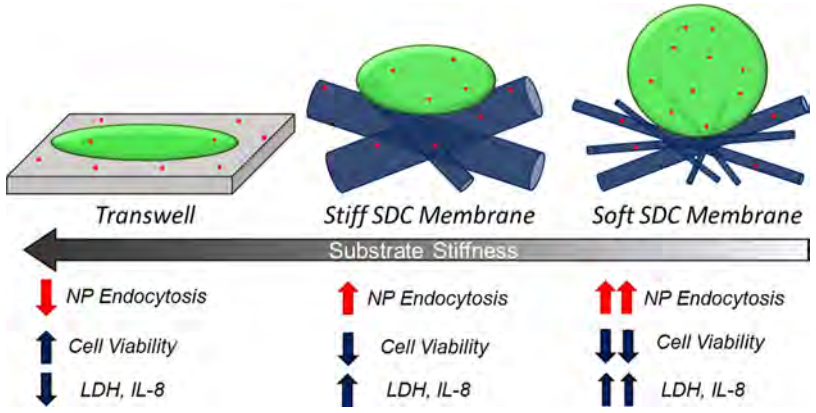

Figure 11. Summary figure providing a pictorial description of the proposed impacts of substrate stiffness on lung epithelial cell nanoparticle endocytosis, viability, and pro-inflammatory cytokine secretion.

these parameters are often overlooked when evaluating toxicity. However, it has been shown that both substrate stiffness and topography impact nanomaterial uptake.[28] Using a blended polydimethylsiloxane (PDMS) model adapted from Plaschenko *et al.*, variable modulus, 2D substrates were developed to study how uptake-efficiency impacts toxicity. Decreasing substrate stiffness increased Ta−Au nanoparticle uptake, directly impacting A_{549} cell viability (Figure S5, 2D substrate stiffness endocytosis results). While this data highlights the importance of biomechanics in toxicological investigations, these conditions lack physiological relevance. The 2D models lack dimensionality and morphological cues representative of human tissue preventing ALI culture for direct aerosol exposure analysis. For this reason, a novel platform that allowed tunable elastic modulus while resembeling native human lung tissue morphology and microstructure was developed. Most importantly, the PU SDC model enabled ALI culture and maintained barrier integrity providing the opportunity to characterize the impact of substrate stiffness in a more physiological context.

Interestingly, no significant difference in Ta−Au uptake was observed for cells cultured on TW under submerged compared to ALI conditions, while nearly 2-fold more particles were uptaken by cells cultured on Soft PU SDCs when cultured at ALI as compared to submerged cell culture (Figure 7). Furthermore, an increase in uptake was observed for cells cultured on soft PU SDC membranes at ALI as compared to those cultured on stiff PU SDC membranes (Figure 7). Endocytosis is a time-dependent process requiring cellular membrane−NM interactions. Taken together, the results from stiff and soft SDC scaffolds indicate that the increased volume of the 3D substrates alone impacted endocytosis, but that substrate stiffness mediated the increase in NM uptake. Indications that cellular membrane thermodynamics dictates the cells ability to endocytose NM, dependent on the shape, size, surface tension, and charge.[42,58,59] Cells have a finite volume of cell membrane placing upper and lower bounds on their cell shape and thus membrane tension.[59] It has been shown that cells cultured on stiff, flat surfaces exhibit maximal cell membrane tension, due to the elongated and stretched cellular morphologies. Cells cultured on softer matrices mimicking their respective tissue of origin results in more spherical, less tense cell membranes. This reduction in cell membrane tension has been theorized to enable greater cellular membrane flexibility, increasing the rate and potential for NM endocytosis.[59] This theory has been explored experimentally using cytoskeletal drugs to inhibit actin remodeling and tubulin interactions, providing soft and stiff cellular models to test NM endocytosis.[37,41,42] While this study did not evaluate novel toxic NMs exposure, the results indicate that cellular responses are impacted strongly by substrate stiffness and culture condition. Common *in vitro* methods lack the design flexibility to mimic human tissue mechanics or microstructure potentially limiting the value and extrapolation potential of NM toxicological evaluations.

Ta−Au nanoparticles are considered bio-inert and thus are commonly used in biological applications such as biosensors due to their biocompatibility.[60] Therefore, in order to evaluate endocytosis efficiency in response to substrate stiffness and culture conditions Ta−Au served as baseline assessment. However, increased Ta−Au NM uptake has been shown to induce cell stress resulting in cell death at high concentrations commonly in excess of 100 μg/mL.[61,62] In this study, we exposed submerged and ALI cultures to 5 μg of Ta−Au NP per TW (4.46 $\mu g/cm^2$), significantly below levels found to be toxic in cell culture. Common *in vitro* models utilizing tissue culture polystyrene (500×10^6 kPa) or polyester TW membranes (1.5×10^6 kPa) are of non-physiological stiffness. Cells cultured on these "ultra-stiff" substrates are notoriously resilient to NM exposures, commonly requiring a super-physiological dosing to achieve biological stress. Likewise, solid tumors are often significantly more stiff than the surrounding "healthy" tissue and have an amazing ability to withstand harsh clinical interventions.[63,64] Further, it is common for biopersistent materials to elicit a foreign body response resulting in fibrosis and stiffening of the tissue.[65] Chronic inflammation and nanomaterial-mediated pulmonary fibrosis drive pathological stiffening of the lung tissue.[66−68] This is likely a protection mechanism, but also limits total lung function and impacts human standard of life. Currently, there no treatments to slow the progression of lung fibrosis or correct damage associated by stiffened lung tissue.[69] Understanding the cellular and molecular impacts of nanomaterials in physiologically relevant tissue matrices that mimic not only the microstructure and morphology but also the passive and applied mechanics will be crucial in discovering novel therapeutic interventions. A_{549} cells cultured on TW membranes and exposed to Ta−Au displayed no significant differences in viability, cytotoxicity, or inflammatory cytokine secretion for both submerged and ALI culture conditions. In contrast, soft and stiff PU SDC scaffolds elastic modulus modeled physiological bulk lung tissue and displayed substrate stiffness dependent cellular responses. Cells cultured on Soft PU

https://doi.org/10.1021/acsami.1c09701
ACS Appl. Mater. Interfaces 2021, 13, 50643−50656

SDCs exhibited a decrease in viability, and increases in cytotoxicity and IL-8 cytokine secretion. Epithelial cell secretion of pro-inflammatory cytokines signals cellular stress and is a good indicator of NM induced stress.[33] A common trend is developing in that stiffness plays a biomechanical role in dictating cellular responses to NM exposures (Figure 11).

5. CONCLUSIONS

Advanced *in vitro* models aim to provide human physiological relevance in a controllable, cost-effective, and tailorable format. The fabrication of engineered substrates for human cell culture requires novel tools that enable fine control over microstructure, morphology, and mechanics. Polyurethane soft dendritic colloid (PU SDC) particles were produced using a novel shearing processing technique driving the formation of nanofibril-based biomaterial mats of desired porosity, open-microstructure, and tunable mechanics. These PU SDC bioscaffolds serve as an ECM surrogate for cellular adhesion, growth, and maturation. Tuning the volumetric loading of the non-solvent phase enabled the formation of material with a wide range of elastic moduli representing human relevant tissue stiffness. The impact of substrate passive mechanical properties, such as elastic modulus, has extensively been shown to impact cellular processes and drive aberrant pathologies. Lung epithelial cells seeded onto soft or stiff PU SDC substrates and common TW inserts were utilized to evaluate the impact of substrate stiffness and cell culture condition on Ta−Au NP exposure. NP endocytosis or uptake is a common phenomenon resulting in toxicological impact. Lung epithelial cell uptake of Ta−Au NPs was increased on PU SDC scaffolds as compared to the "ultra-stiff" TW insert membranes, resulting in cytotoxicity and inflammatory cytokine secretion. Additionally, we show that culturing A_{549} cells at ALI compared to submerged conditions further impacted cellular endocytosis, viability, and cytokine secretion. Taken together, these results suggest that bioscaffold stiffness, representing human tissues resulted in greater NM endocytosis and resulting toxicological impact. While common *in vitro* methods utilize non-physiologically stiff cell culture substrates, here, we present a biomaterial capable of better representing human tissue with the aim of creating physiologically relevant tissue models for NM toxicological assessment and other biological evaluations. Future evaluation of novel polymer materials and processing techniques will be employed to drive the elastic moduli of the scaffolds down, decrease pore size, and render a thinner mat. Incorporation of paramagnetic nanoparticles within the "core" of PU SDC fibrils[52] could provide a means to apply active mechanical properties emulating human breathing (Supporting Information Video S10, magnetic actuation of PU SDC scaffolds containing a 3D printed iron oxide nanoparticle doped PDMS backbone), model gut peristalsis, or muscle contraction forces, further improving the physiological relevance and closing the gap between laboratory and *in vivo* models.

DATA AVAILABILITY

All data presented are available upon request from the corresponding author.

ASSOCIATED CONTENT

Supporting Information

The Supporting Information is available free of charge at https://pubs.acs.org/doi/10.1021/acsami.1c09701.

Vitrocell cloud deposition optimization, total A549 cell count on TW and PU SDC scaffolds in submerged and ALI conditions, paracellular transport of a fluorescent indicator Cascade blue, IL-8 ELISA control exposures using LPS, and workflow for the development of 2D variable modulus substrates (PDF)

Video S6: 3D reconstructed confocal z-stack, 20x A549 on stiff PU SDC (MP4)

Video S7: 3D reconstructed confocal z-stack, 20x A549 on soft PU SDC (MP4)

Video S8: 3D reconstructed confocal z-stack, 40x A549 on soft PU SDC (MP4)

Video S9: 3D micro-CT video of soft and stiff PU SDC scaffolds (MP4)

Video S10: magnetic actuation of PU SDC scaffolds containing a 3D printed iron oxide nanoparticle doped PDMS backbone (MP4)

AUTHOR INFORMATION

Corresponding Authors

Orlin D. Velev − *Department of Chemical and Biomolecular Engineering, North Carolina State University, Raleigh, North Carolina 27695, United States*; Email: odvelev@ncsu.edu

M. Tyler Nelson − *Air Force Research Laboratory, Wright-Patterson AFB, Ohio 45433, United States*; orcid.org/0000-0002-7255-4964; Email: mark.nelson.35@us.af.mil

Authors

Austin H. Williams − *Department of Chemical and Biomolecular Engineering, North Carolina State University, Raleigh, North Carolina 27695, United States*; orcid.org/0000-0003-4080-5164

Adrien M. Hebert − *Air Force Research Laboratory, Wright-Patterson AFB, Ohio 45433, United States*

Robert C. Boehm − *Air Force Research Laboratory, Wright-Patterson AFB, Ohio 45433, United States*

Mary E. Huddleston − *Air Force Research Laboratory, Wright-Patterson AFB, Ohio 45433, United States; UES, Inc., Dayton, Ohio 45432, United States*

Meghan R. Jenkins − *Air Force Research Laboratory, Wright-Patterson AFB, Ohio 45433, United States; UES, Inc., Dayton, Ohio 45432, United States*

Complete contact information is available at: https://pubs.acs.org/10.1021/acsami.1c09701

Author Contributions

Development, design, and characterization of membrane materials were performed by A.H.W and O.D.V.; experimental design of cell viability and response was performed by A.M.H., R.C.B., and M.T.N.; data were analyzed by M.T.N., A.H.W., and O.D.V.; M.E.H. and M.R.J. imaged and provided permeability results; the manuscript was written by A.H.W. and M.T.N. with edits by O.D.V. and M.T.N., and reviewed by all authors.

Funding

This work was funded by the 711th Human Performance Wing, Chief Scientist Fiscal Year 19 Seedling Grant. We acknowledge partial support from NSF grant CMMI—1825476.

Notes

The authors declare no competing financial interest.

■ ACKNOWLEDGMENTS

The authors thank Dr. Michael Dickey for the use of his group's equipment for the mechanical analysis.

■ REFERENCES

(1) Silvani, S.; Figliuzzi, M.; Remuzzi, A. Toxicological Evaluation of Airborne Particulate Matter. Are Cell Culture Technologies Ready to Replace Animal Testing ? *J. Appl. Toxicol.* **2019**, *39*, 1484.
(2) Biswas, P.; Wu, C. Y. Nanoparticles and the Environment. *J. Air Waste Manage. Assoc.* **2005**, *55*, 708−746.
(3) Stone, V.; Miller, M. R.; Clift, M. J. D.; Elder, A.; Mills, N. L.; Møller, P.; Schins, R. P. F.; Vogel, U.; Kreyling, W. G.; Jensen, K. A.; Kuhlbusch, T. A. J.; Schwarze, P. E.; Hoet, P.; Pietroiusti, A.; de Vizcaya-Ruiz, A.; Baeza-Squiban, A.; Teixeira, J. P.; Tran, C. L.; Cassee, F. R. Nanomaterials versus Ambient Ultrafine Particles: An Opportunity to Exchange Toxicology Knowledge. *Environ. Health Perspect.* **2017**, *125*, 106002.
(4) Schraufnagel, D. E. The Health Effects of Ultrafine Particles. *Exp. Mol. Med.* **2020**, *52*, 311−317.
(5) Deloid, G. M.; Cohen, J. M.; Pyrgiotakis, G.; Demokritou, P. Preparation, Characterization, and in Vitro Dosimetry of Dispersed, Engineered Nanomaterials. *Nat. Protoc.* **2017**, *12*, 355−371.
(6) Cohen, J. M.; Teeguarden, J. G.; Demokritou, P. An integrated approach for the in vitro dosimetry of engineered nanomaterials. *Part. Fibre Toxicol.* **2014**, *11*, 20.
(7) Deloid, G.; Cohen, J. M.; Darrah, T.; Derk, R.; Rojanasakul, L.; Pyrgiotakis, G.; Wohlleben, W.; Demokritou, P. Estimating the Effective Density of Engineered Nanomaterials for in Vitro Dosimetry. *Nat. Commun.* **2014**, *5*, 3514.
(8) Cohen, J.; DeLoid, G.; Pyrgiotakis, G.; Demokritou, P. Interactions of engineered nanomaterials in physiological media and implications forin vitrodosimetry. *Nanotoxicology* **2013**, *7*, 417−431.
(9) Cohen, J. M.; DeLoid, G. M.; Demokritou, P. A Critical Review of in Vitro Dosimetry for Engineered Nanomaterials. *Nanomedicine* **2015**, *10*, 3015−3032.
(10) Herzog, F.; Loza, K.; Balog, S.; Clift, M. J. D.; Epple, M.; Gehr, P.; Petri-Fink, A.; Rothen-Rutishauser, B. Mimicking Exposures to Acute and Lifetime Concentrations of Inhaled Silver Nanoparticles by Two Different in Vitro Approaches. *Beilstein J. Nanotechnol.* **2014**, *5*, 1357−1370.
(11) Tilly, T. B.; Nelson, M. T.; Chakravarthy, K. B.; Shira, E. A.; Debrose, M. C.; Grabinski, C. M.; Salisbury, R. L.; Mattie, D. R.; Hussain, S. M. In Vitro Aerosol Exposure to Nanomaterials: From Laboratory to Environmental Field Toxicity Testing. *Chem. Res. Toxicol.* **2020**, *33*, 1179−1194.
(12) Paur, H.-R.; Cassee, F. R.; Teeguarden, J.; Fissan, H.; Diabate, S.; Aufderheide, M.; Kreyling, W. G.; Hänninen, O.; Kasper, G.; Riediker, M.; Rothen-Rutishauser, B.; Schmid, O. In-Vitro Cell Exposure Studies for the Assessment of Nanoparticle Toxicity in the Lung-A Dialog between Aerosol Science and Biology. *J. Aerosol Sci.* **2011**, *42*, 668−692.
(13) Hussain, S. M.; Warheit, D. B.; Ng, S. P.; Comfort, K. K.; Grabinski, C. M.; Braydich-Stolle, L. K. At the Crossroads of Nanotoxicologyin vitro: Past Achievements and Current Challenges. *Toxicol. Sci.* **2015**, *147*, 5−16.
(14) Huang, D.; Liu, T.; Liao, J.; Maharjan, S.; Xie, X.; Pérez, M.; Anaya, I.; Wang, S.; Tirado Mayer, A.; Kang, Z.; Kong, W.; Mainardi, V. L.; Garciamendez-Mijares, C. E.; García Martínez, G.; Moretti, M.; Zhang, W.; Gu, Z.; Ghaemmaghami, A. M.; Zhang, Y. S. Reversed-Engineered Human Alveolar Lung-on-a-Chip Model. *Proc. Natl. Acad. Sci.* **2021**, *118*, No. e2016146118.
(15) Gordon, S.; Daneshian, M.; Bouwstra, J.; Caloni, F.; Constant, S.; Davies, D. E.; Dandekar, G.; Guzman, C. A.; Fabian, E.; Haltner, E.; Hartung, T.; Hasiwa, N.; Hayden, P.; Kandarova, H.; Khare, S.; Krug, H. F.; Kneuer, C.; Leist, M.; Lian, G.; Marx, U.; Metzger, M.; Ott, K.; Prieto, P.; Roberts, M. S.; Roggen, E. L.; Tralau, T.; Van Den Braak, C.; Walles, H.; Lehr, C. M. Non-Animal Models of Epithelial Barriers (Skin, Intestine and Lung) in Research, Industrial Applications and Regulatory Toxicology. *Altex* **2015**, *32*, 327−378.
(16) Klein, S. G.; Serchi, T.; Hoffmann, L.; Blömeke, B.; Gutleb, A. C. An Improved 3D Tetraculture System Mimicking the Cellular Organisation at the Alveolar Barrier to Study the Potential Toxic Effects of Particles on the Lung. *Part. Fibre Toxicol.* **2013**, *10*, 31.
(17) Patel, B.; Gauvin, R.; Absar, S.; Gupta, V.; Gupta, N.; Nahar, K.; Khademhosseini, A.; Ahsan, F. Computational and Bioengineered Lungs as Alternatives to Whole Animal, Isolated Organ, and Cell-Based Lung Models. *Am. J. Physiol.: Lung Cell. Mol. Physiol.* **2012**, *303*, L733−L747.
(18) Artzy-Schnirman, A.; Hobi, N.; Schneider-Daum, N.; Guenat, O. T.; Lehr, C.-M.; Sznitman, J. Advanced in Vitro Lung-on-Chip Platforms for Inhalation Assays: From Prospect to Pipeline. *Eur. J. Pharm. Biopharm.* **2019**, *144*, 11−17.
(19) Luyts, K.; Napierska, D.; Dinsdale, D.; Klein, S. G.; Serchi, T.; Hoet, P. H. M. A coculture model of the lung-blood barrier: The role of activated phagocytic cells. *Toxicol. In Vitro* **2015**, *29*, 234−241.
(20) Nichols, J. E.; Niles, J. A.; Vega, S. P.; Argueta, L. B.; Eastaway, A.; Cortiella, J. Modeling the Lung: Design and Development of Tissue Engineered Macro- and Micro-Physiologic Lung Models for Research Use. *Exp. Biol. Med.* **2014**, *239*, 1135−1169.
(21) Tenenbaum-Katan, J.; Artzy-Schnirman, A.; Fishler, R.; Korin, N.; Sznitman, J. Biomimetics of the Pulmonary Environment in Vitro: A Microfluidics Perspective. *Biomicrofluidics* **2018**, *12*, 042209.
(22) Ghadiali, S. N.; Gaver, D. P. Biomechanics of Liquid-Epithelium Interactions in Pulmonary Airways. *Respir. Physiol. Neurobiol.* **2008**, *163*, 232−243.
(23) Wong, J. Y.; Leach, J. B.; Brown, X. Q. Balance of Chemistry, Topography, and Mechanics at the Cell-Biomaterial Interface: Issues and Challenges for Assessing the Role of Substrate Mechanics on Cell Response. *Surf. Sci.* **2004**, *570*, 119−133.
(24) Winter, J. O.; Calhoun, M. A.; Bentil, S.; Short, A.; Nelson, T.; Sarkar, A.; Lannuti, J. J.; Dupaix, R. Beyond Elastic Modulus: The Role of Interfacial Mechanics in Cell Behavior. *Surf. Sci.* **2013**, *570*, 119−133.
(25) Brown, S. C.; Kamal, M.; Nasreen, N.; Baumuratov, A.; Sharma, P.; Antony, V. B.; Moudgil, B. M. Influence of shape, adhension and simulated lung mechanics on amorphous silica nanoparticle toxicity. *Adv. Powder Technol.* **2007**, *18*, 69−79.
(26) Guenat, O. T.; Berthiaume, F. Incorporating Mechanical Strain in Organs-on-a-Chip: Lung and Skin. *Biomicrofluidics* **2018**, *12*, 042207.
(27) Artzy-Schnirman, A.; Arber Raviv, S.; Doppelt Flikshtain, O.; Shklover, J.; Korin, N.; Gross, A.; Mizrahi, B.; Schroeder, A.; Sznitman, J. Advanced Human-Relevant in Vitro Pulmonary Platforms for Respiratory Therapeutics. *Adv. Drug Delivery Rev.* **2021**, *176*, 113901.
(28) Palchesko, R. N.; Zhang, L.; Sun, Y.; Feinberg, A. W. Development of Polydimethylsiloxane Substrates with Tunable Elastic Modulus to Study Cell Mechanobiology in Muscle and Nerve. *PLoS One* **2012**, *7*, No. e51499.
(29) Boomer, L.; Liu, Y.; Mahler, N.; Johnson, J.; Zak, K.; Nelson, T.; Lannutti, J.; Besner, G. E. Scaffolding for Challenging Environments: Materials Selection for Tissue Engineered Intestine. *J. Biomed. Mater. Res., Part A* **2014**, *102*, 3795−3802.
(30) Luque, T.; Melo, E.; Garreta, E.; Cortiella, J.; Nichols, J.; Farré, R.; Navajas, D. Local Micromechanical Properties of Decellularized Lung Scaffolds Measured with Atomic Force Microscopy. *Acta Biomater.* **2013**, *9*, 6852−6859.
(31) Ameer, J. M.; Anil Kumar, P. R.; Kasoju, N. Strategies to Tune Electrospun Scaffold Porosity for Effective Cell Response in Tissue Engineering. *J. Funct. Biomater.* **2019**, *10*, 30.
(32) Pizzo, A. M.; Kokini, K.; Vaughn, L. C.; Waisner, B. Z.; Voytik-Harbin, S. L. Extracellular Matrix (ECM) Microstructural Composition Regulates Local Cell-ECM Biomechanics and Fundamental Fibroblast Behavior: A Multidimensional Perspective. *J. Appl. Physiol.* **2005**, *98*, 1909−1921.
(33) Jeon, H.; Tsui, J. H.; Jang, S. I.; Lee, J. H.; Park, S.; Mun, K.; Boo, Y. C.; Kim, D.-H. Combined Effects of Substrate Topography and Stiffness on Endothelial Cytokine and Chemokine Secretion. *ACS Appl. Mater. Interfaces* **2015**, *7*, 4525−4532.
(34) Truby, R. L.; Lewis, J. A. Printing Soft Matter in Three Dimensions. *Nature* **2016**, *540*, 371−378.

https://doi.org/10.1021/acsami.1c09701
ACS Appl. Mater. Interfaces 2021, 13, 50643−50656

(35) Mitchell, G. R.; Tojeira, A. Role of Anisotropy in Tissue Engineering. *Procedia Eng* **2013**, *59*, 117−125.
(36) Chen, S.; John, J. V.; Mccarthy, A.; Carlson, M. A.; Li, X.; Xie, J. Fast transformation of 2D nanofiber membranes into pre-molded 3D scaffolds with biomimetic and oriented porous structure for biomedical applications. *Appl. Phys. Rev.* **2020**, *7*, 021406.
(37) Huang, C.; Ozdemir, T.; Xu, L.-C.; Butler, P. J.; Siedlecki, C. A.; Brown, J. L.; Zhang, S. The Role of Substrate Topography on the Cellular Uptake of Nanoparticles. *J. Biomed. Mater. Res., Part B* **2016**, *104*, 488−495.
(38) Ataollahi, F.; Pramanik, S.; Moradi, A.; Dalilottojari, A.; Pingguan-Murphy, B.; Wan Abas, W. A. B.; Abu Osman, N. A. Endothelial Cell Responses in Terms of Adhesion, Proliferation, and Morphology to Stiffness of Polydimethylsiloxane Elastomer Substrates. *J. Biomed. Mater. Res., Part A* **2015**, *103*, 2203−2213.
(39) Sun, M.; Chi, G.; Li, P.; Lv, S.; Xu, J.; Xu, Z.; Xia, Y.; Tan, Y.; Xu, J.; Li, L.; Li, Y. Effects of Matrix Stiffness on the Morphology, Adhesion, Proliferation and Osteogenic Differentiation of Mesenchymal Stem Cells. *Int. J. Med. Sci.* **2018**, *15*, 257−268.
(40) Xu, Q.; Li, C.; Kang, Y.; Zhang, Y. Long Term Effects of Substrate Stiffness on the Development of HMSC Mechanical Properties. *RSC Adv.* **2015**, *5*, 105651−105660.
(41) Barker, T. H.; Dysart, M. M.; Brown, A. C.; Douglas, A. M.; Fiore, V. F.; Russell, A. G. *Synergistic Effects of Particulate Matter and Substrate Stiffness on Epithelial-To-Mesenchymal Transition*; Health Effects Institute, 2014.
(42) Huang, C.; Butler, P. J.; Tong, S.; Muddana, H. S.; Bao, G.; Zhang, S. Substrate Stiffness Regulates Cellular Uptake of Nanoparticles. *Nano Lett.* **2013**, *13*, 1611−1615.
(43) Bitterle, E.; Karg, E.; Schroeppel, A.; Kreyling, W. G.; Tippe, A.; Ferron, G. A.; Schmid, O.; Heyder, J.; Maier, K. L.; Hofer, T. Dose-Controlled Exposure of A549 Epithelial Cells at the Air-Liquid Interface to Airborne Ultrafine Carbonaceous Particles. *Chemosphere* **2006**, *65*, 1784−1790.
(44) Melo, E.; Cárdenes, N.; Garreta, E.; Luque, T.; Rojas, M.; Navajas, D.; Farré, R. Inhomogeneity of Local Stiffness in the Extracellular Matrix Scaffold of Fibrotic Mouse Lungs. *J. Mech. Behav. Biomed. Mater.* **2014**, *37*, 186−195.
(45) Nelson, M. T.; Short, A.; Cole, S. L.; Gross, A. C.; Winter, J.; Eubank, T. D.; Lannutti, J. J. Preferential, enhanced breast cancer cell migration on biomimetic electrospun nanofiber "cell highways". *BMC Cancer* **2014**, *14*, 825.
(46) Cidem, A.; Bradbury, P.; Traini, D.; Ong, H. X. Modifying and Integrating in Vitro and Ex Vivo Respiratory Models for Inhalation Drug Screening. *Front. Bioeng. Biotechnol.* **2020**, *8*, 581995.
(47) Roh, S.; Williams, A. H.; Bang, R. S.; Stoyanov, S. D.; Velev, O. D. Soft Dendritic Microparticles with Unusual Adhesion and Structuring Properties. *Nat. Mater.* **2019**, *18*, 1315−1320.
(48) Alargova, R. G.; Bhatt, K. H.; Paunov, V. N.; Velev, O. D. Scalable Synthesis of a New Class of Polymer Microrods by a Liquid-Liquid Dispersion Technique. *Adv. Mater.* **2004**, *16*, 1653−1657.
(49) Smoukov, S. K.; Tian, T.; Vitchuli, N.; Gangwal, S.; Geisen, P.; Wright, M.; Shim, E.; Marquez, M.; Fowler, J.; Velev, O. D. Scalable Liquid Shear-Driven Fabrication of Polymer Nanofibers. *Adv. Mater.* **2015**, *27*, 2642−2647.
(50) Scotti, A.; Meneveau, C. A Fractal Model for Large Eddy Simulation of Turbulent Flow. *Phys. D* **1999**, *127*, 198−232.
(51) Alkindi, A. S.; Al-Wahaibi, Y. M.; Muggeridge, A. H. Physical Properties (Density, Excess Molar Volume, Viscosity, Surface Tension, and Refractive Index) of Ethanol + Glycerol. *J. Chem. Eng. Data* **2008**, *53*, 2793−2796.
(52) Caliari, S. R.; Harley, B. A. C. The Effect of Anisotropic Collagen-GAG Scaffolds and Growth Factor Supplementation on Tendon Cell Recruitment, Alignment, and Metabolic Activity. *Biomaterials* **2011**, *32*, 5330−5340.
(53) Zhao, G.; Zhang, X.; Lu, T. J.; Xu, F. Recent Advances in Electrospun Nanofibrous Scaffolds for Cardiac Tissue Engineering. *Adv. Funct. Mater.* **2015**, *25*, 5726−5738.
(54) Araujo, J.; Padrão, J.; Silva, J. P.; Dourado, F.; Correia, D. M.; Botelho, G.; Gomez Ribelles, J. L.; Lanceros-Méndez, S.; Sencadas, V. Processing and characterization of α-elastin electrospun membranes. *Appl. Phys. A: Mater. Sci. Process.* **2014**, *115*, 1291−1298.
(55) Kumbar, S. G.; James, R.; Nukavarapu, S. P.; Laurencin, C. T. Electrospun Nanofiber Scaffolds: Engineering Soft Tissues. *Biomed. Mater.* **2008**, *3*, 034002.
(56) Freed, L. E.; Engelmayr, G. C., Jr; Borenstein, J. T.; Moutos, F. T.; Guilak, F. Advanced Material Strategies for Tissue Engineering Scaffolds. *Adv. Mater.* **2009**, *21*, 3410−3418.
(57) Morris, G. E.; Bridge, J. C.; Eltboli, O. M. I.; Knox, A. J.; Aylott, J. W.; Brightling, C. E.; Ghaemmaghami, A. M.; Rose, F. R. A. J. Human Airway Smooth Muscle Maintain in Situ Cell Orientation and Phenotype When Cultured on Aligned Electrospun Scaffolds. *Am. J. Physiol.: Lung Cell. Mol. Physiol.* **2014**, *307*, L38−L47.
(58) Geiser, M.; Rothen-Rutishauser, B.; Kapp, N.; Schürch, S.; Kreyling, W.; Schulz, H.; Semmler, M.; Hof, V. I.; Heyder, J.; Gehr, P. Ultrafine Particles Cross Cellular Membranes by Nonphagocytic Mechanisms in Lungs and in Cultured Cells. *Environ. Health Perspect.* **2005**, *113*, 1555−1560.
(59) Zhang, S.; Gao, H.; Bao, G. Physical Principles of Nanoparticle Cellular Endocytosis. *ACS Nano* **2015**, *9*, 8655−8671.
(60) German, N.; Ramanavicius, A.; Voronovic, J.; Ramanaviciene, A. Glucose Biosensor Based on Glucose Oxidase and Gold Nanoparticles of Different Sizes Covered by Polypyrrole Layer. *Colloids Surf., A* **2012**, *413*, 224−230.
(61) Chithrani, B. D.; Ghazani, A. A.; Chan, W. C. W. Determining the Size and Shape Dependence of Gold Nanoparticle Uptake into Mammalian Cells. *Nano Lett.* **2006**, *6*, 662−668.
(62) Fytianos, K.; Chortarea, S.; Rodriguez-Lorenzo, L.; Blank, F.; Von Garnier, C.; Petri-Fink, A.; Rothen-Rutishauser, B. Aerosol Delivery of Functionalized Gold Nanoparticles Target and Activate Dendritic Cells in a 3D Lung Cellular Model. *ACS Nano* **2017**, *11*, 375−383.
(63) Shieh, A. C. Biomechanical Forces Shape the Tumor Microenvironment. *Ann. Biomed. Eng.* **2011**, *39*, 1379−1389.
(64) Zustiak, S. P.; Dadhwal, S.; Medina, C.; Steczina, S.; Chehreghanianzabi, Y.; Ashraf, A.; Asuri, P. Three-Dimensional Matrix Stiffness and Adhesive Ligands Affect Cancer Cell Response to Toxins. *Biotechnol. Bioeng.* **2016**, *113*, 443−452.
(65) Cho, W. S.; Duffin, R.; Howie, S. E.; Scotton, C. J.; Wallace, W. A.; MacNee, W.; Bradley, M.; Megson, I. L.; Donaldson, K. Progressive Severe Lung Injury by Zinc Oxide Nanoparticles; the Role of Zn2+dissolution inside Lysosomes. *Part. Fibre Toxicol.* **2011**, *8*, 27.
(66) Monteiller, C.; Tran, L.; Macnee, W.; Faux, S.; Jones, A.; Miller, B.; Donaldson, K. The Pro-Inflammatory Effects of Low-Toxicity Low-Solubility Particles, Nanoparticles and Fine Particles, on Epithelial Cells in Vitro: The Role of Surface Area. *Occup. Environ. Med.* **2007**, *64*, 609−615.
(67) Ma, J. Y.; Mercer, R. R.; Barger, M.; Schwegler-berry, D.; Scabilloni, J.; Ma, J. K.; Castranova, V. Induction of pulmonary fibrosis by cerium oxide nanoparticles. *Toxicol. Appl. Pharmacol.* **2012**, *262*, 255−264.
(68) Song, Y.; Li, X.; Du, X. Exposure to Nanoparticles Is Related to Pleural Effusion, Pulmonary Fibrosis and Granuloma. *Eur. Respir. J.* **2009**, *34*, 559−567.
(69) Sun, B.; Shi, Y.; Li, Y.; Jiang, J.; Liang, S.; Duan, J.; Sun, Z. Short-term PM2.5 exposure induces sustained pulmonary fibrosis development during post-exposure period in rats. *J. Hazard. Mater.* **2020**, *385*, 121566.

https://doi.org/10.1021/acsami.1c09701
ACS Appl. Mater. Interfaces 2021, 13, 50643−50656